

OrthographicNet: A Deep Learning Approach for 3D Object Recognition in Open-Ended Domains

S. Hamidreza Kasaei

Dept. of Artificial Intelligence, University of Groningen, Groningen, The Netherlands.

Email: hamidreza.kasaei@rug.nl

Abstract—Service robots are expected to be more autonomous and efficiently work in human-centric environments. For this type of robots, open-ended object recognition is a challenging task due to the high demand for two essential capabilities: (i) the accurate and real-time response, and (ii) the ability to learn new object categories from very few examples on-site. These capabilities are required for such robots since no matter how extensive the training data used for batch learning, the robot might be faced with an *unknown* object when operating in everyday environments. In this work, we present *OrthographicNet*, a deep transfer learning based approach, for 3D object recognition in open-ended domains. In particular, *OrthographicNet* generates a rotation and scale invariant global feature for a given object, enabling to recognize the same or similar objects seen from different perspectives. Experimental results show that our approach yields significant improvements over the previous state-of-the-art approaches concerning scalability, memory usage and object recognition performance. Regarding real-time performance, two real-world demonstrations validate the promising performance of the proposed architecture. Moreover, our approach demonstrates the capability of learning from very few training examples in a real-world setting.

I. INTRODUCTION

Nowadays robots utilize 3D computer vision algorithms to perform complex tasks such as object recognition and manipulation. Although many problems have already been understood and solved successfully, many issues still remain. *Open-ended object recognition* is one of these issues waiting for many improvements. In particular, most robots cannot learn new object categories using on-site experiences. In open-ended domains the set of categories to be learned is not predefined in advance. Therefore, it is not feasible to assume that one can pre-program all possible object categories and anticipate all exceptions for robots. Instead, robots should learn autonomously from novel experiences, supported in the feedback from human teachers. This way, it is expected that the competence of the robot increases over time. To address this problem, the *learning system* of the robots should have four characteristics:

- **On-line**: meaning that the learning procedure takes place while the robot is running.
- **Supervised**: to include the human instructor in the learning process. This is an effective way for a robot to obtain knowledge from a human teacher.
- **Incremental**: it is able to adjust the learned model of a certain category when a new instance is taught.
- **Opportunistic**: apart from learning from a batch of

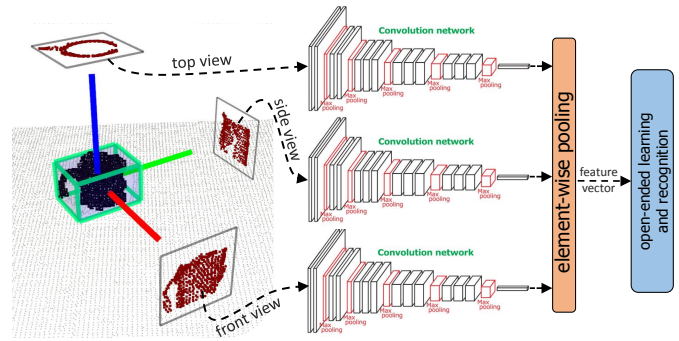


Fig. 1. Overview of the proposed open-ended object recognition pipeline: (left) the *cup* object and its bounding box, reference frame and three projected views; (center) each orthographic projection is then fed to a CNN to obtain a view-wise deep feature; (right) to construct a global deep representation for the given object, view-wise features are merged using an element-wise pooling function. The obtained representation is finally used for open-ended learning and recognition.

labelled training data at predefined times or according to a predefined training schedule, the robot must be prepared to accept a new example when it becomes available.

This paper presents an interactive open-ended learning approach for 3D object recognition. In this work, “*open-ended*” means that the robot does not know in advance which object categories it will have to learn, which observations will be available, and when they will be available to support the learning. Most of the recent approaches use Convolutional Neural Networks (CNN) for 3D object recognition [10, 33, 40, 39, 31]. It is now clear that if an application has a pre-defined fixed set of object categories and thousands of examples per category, an effective way to build an object recognition system is to train a deep CNN. However, there are several limitations to use CNN in open-ended domains. CNNs are incremental by nature but not open-ended, since the inclusion of new categories enforces a restructuring in the topology of the network. Moreover, CNNs usually need a lot of training data and if limited training data is used, this might lead to non-discriminative object representations and, as a consequence, to poor object recognition performance. Deep transfer learning can relax these limitations and motivates us to combine deep-learned features with an online classifier to handle the problem of open-ended object category learning and recognition.

In this paper, we propose a deep transfer learning based approach for 3D object recognition in open-ended domains.

To the best of our knowledge, there is no other deep transfer learning approach jointly tackling 3D object pose estimation and recognition in open-ended fashion. As depicted in Fig. 1, we first construct a unique reference frame for the given object. Afterwards, three principal orthographic projections including *front*, *top*, and *right-side* views are computed by exploiting the object reference frame. Each projected view is then fed to a CNN to obtain a view-wise deep feature. The obtained view-wise features are then merged, using an element-wise max-pooling function, to construct a global feature for the given object. The obtained global feature is scale and pose invariant, informative and stable, and designed with the objective of supporting accurate 3D object recognition. We finally conducted our experiments with an instance-based learning and a nearest-neighbor classification rule.

The remainder of this paper is organized as follows: Section II reviews related work of open-ended learning and deep learning approaches applied to 3D object recognition. Next, the detailed methodologies of our proposal – namely *OrthographicNet* – are explained in Section III and IV. Experimental result and discussion are given in Section V, followed by conclusions in Section VI.

II. RELATED WORK

In the last decade, various research groups have made substantial progress towards the development of learning approaches which support online and incremental object category learning [18, 17, 9, 19, 25]. In such systems, *object representation* plays a prominent role since its output is used in both learning and recognition phases. Furthermore, it must provide reliable information in real-time to enable the robot to physically interact with the objects. Therefore, building a discriminative object representation is a challenging step to improve object recognition performance.

In [18], an open-ended object category learning system, based on a global 3D shape feature namely GOOD [16], is described. In particular, the authors proposed a cognitive robotic architecture to create a concurrent 3D object category learning and recognition in an interactive and open-ended manner. Kasaei et al. [17] proposed a naive Bayes learning approach with a Bag-of-Words object representation to acquire and refine object category models in open-ended fashion. Faulhammer et al. [9] presented a system which allows a mobile robot to autonomously detect, model and recognize objects in everyday environments. Skocaj et al. [34] presented an integrated robotic system capable of interactive learning in dialogue with a human. Their system learns and refines conceptual models of visual objects and their properties, either by attending to information provided by a human tutor or by taking initiative itself. For the object recognition purpose, they mainly used two hand-crafted features including SIFT [22] (texture-based) as well as SHOT [28] (shape-based) descriptors. Oliveira et al. [24] tackle this problem by proposing an approach for concurrent learning of visual code-books and object categories in open-ended domains. Aldoma et al. [1] reviewed properties, advantages and disadvantages of

several state-of-the-art 3D shape descriptors available from the Point Cloud Library (PCL) to develop 3D object recognition and pose estimation system. All the above approaches use hand-crafted features. This in turn means that they may not generalize well across different domains.

Recently, deep learning approaches have received significant attention from the robotics, machine learning, and computer vision communities. Deep learning methods have shown superior performance compared with the 3D hand-craft descriptors. For 3D object recognition, deep learning approaches can be categorized into three categories according to their input: (i) volume-based [39, 40, 23], (ii) view-based [31, 33, 35], and (iii) pointset-based methods [10, 27, 20]. Volume-based approaches, first represent an object as a 3D voxel grid and then use the obtained representation as the input to a CNN with 3D filter banks. Approaches of the second category (i.e., view-based) extract 2D images from the 3D representation by projecting the object’s points into 2D planes. In contrast, pointset-based approaches work directly on 3D point clouds and require neither voxelization nor projecting 3D points into multiple 2D views. Among these methods, experiments indicate that view-based methods have performed best in object recognition so far [26].

Wu et al. [39] proposed a volume-based approach for 3D object recognition namely ShapeNets. In this work, the authors mainly extended the AlexNet architecture from 2D convolutions to 3D convolutions. ShapeNets first categorized each voxel of an object as free space, surface or occluded, depending on whether it is in front of, on, or behind the visible surface from the depth map and then fed the obtained representation into the extended 3D CNN. Maturana et al. [23] proposed a similar approach namely VoxNet, which uses binary voxel grids representation and a CNN architecture. Xu and Todorovic [40] formulated CNN learning for 3D object recognition as a beam search aimed at identifying an optimal CNN architecture as well as estimating optimal parameters for the CNN (here referred to as BeamNet). In contrast, view-based methods try to exploit established 2D CNN architectures. Shi et al. [31] tackle the problem of 3D object recognition by combining a panoramic representation of 3D objects with a CNN, i.e., named DeepPano. In this approach, each object is first converted into a panoramic view, i.e., a cylinder projection object around its principle axis. Then, a variant of CNN is used to learn the deep representations from the panoramic views. Su et al. [35] described a object recognition approach based on projecting a 3D object into multiple views and extracting view-wise CNN features. Finally they generate a global representation for the given object by merging all CNN features using an element-wise max-pooling function. In another work, Sinha et al. [33] adopted an approach of converting the 3D object into a “geometry image” and used standard CNNs directly to learn 3D shape surfaces. Our work is also classified as a view-based approaches.

The pointset-based approaches are completely different from the other two. PointNet proposed by Qi et al. [10] directly takes unordered point sets as inputs. PointNet learns a global

representation of a point cloud based on computing individual point features from per-point Multi-Layer-Perceptron (MLP) first and then aggregating all features of the given object. Recently Qi et al. [27] improved PointNet by exploiting local structures induced by the metric space. In particular, PointNet++ segments a point cloud into smaller clusters, and then send each cluster through a small PointNet. Of course, this leads to a complicated architecture with reduced speed and not suitable for real-time application. In another work, Klovov et.al [20] proposed Kd-Networks for the recognition of 3D object represented by 3D point cloud. We compare our method with state-of-the-art deep learning methods including 3DShapeNet [39], DeepPano [31], BeamNet [40], Geometry-Image [33], and PointNet [10].

We also investigate the ability to learn novel classes quickly, which is formulated as a transfer learning problem. Recent deep transfer learning approaches assumed that large amounts of training data are available for novel classes [29]. For such situations the strength of pre-trained CNNs for extracting features is well known [29, 30]. Unlike our approach, CNN-based approaches are not scale and rotation invariant. Several researchers try to solve the issue qualitatively using data augmentation either using Generative Adversarial Networks (GAN) [11] or by modifying images by translation, flipping, rotating and adding noise [38] i.e., CNNs are still required to learn the rotation equivariance properties from the data [7, 6]. Furthermore, unlike these CNN-based approaches, we assume that the training instances are extracted from on-site experiences of a robot, and thus become gradually available over time, rather than being completely or partially available at the beginning of the learning process. Moreover, in our approach the set of classes is continuously growing while in the mentioned deep transfer learning approaches the set of classes is predefined.

III. OBJECT REPRESENTATION

A point cloud of an object is represented as a set of points, $\mathbf{p}_i : i \in \{1, \dots, n\}$, where each point is described by their 3D coordinates $[x, y, z]$ and RGB information. As shown in Fig. 1, OrthographicNet starts with constructing a *global object reference frame* (RF) for the given object, since the repeatability of the object reference frame directly affects the descriptiveness of the object representation. Furthermore, a global object descriptor should be invariant to translations, rotations and robust to noise. We call it *global object reference frame* to distinguish it from the reference frame used for computing local features. Towards this end, three principal axes of a given object's point cloud are constructed based on eigenvectors analysis. In particular, we first compute the geometric center of the object using $\mathbf{c} = \frac{1}{n} \sum_{i=1}^n \mathbf{p}_i$. Afterwards, the normalized covariance matrix, Σ , of the object is calculated by $\Sigma = \frac{1}{n} \sum_{i=1}^n (\mathbf{p}_i - \mathbf{c})(\mathbf{p}_i - \mathbf{c})^T$. Then, eigenvalue decomposition is performed on the Σ :

$$\Sigma \mathbf{V} = \mathbf{E} \mathbf{V}, \quad (1)$$

where $\mathbf{V} = [\vec{v}_1, \vec{v}_2, \vec{v}_3]$ is eigenvectors of Σ , and $\mathbf{E} = [\lambda_1, \lambda_2, \lambda_3]$ is the corresponding eigenvalues and $\lambda_1 \geq \lambda_2 \geq \lambda_3$. In other words, the largest eigenvector, \vec{v}_1 , of the covariance matrix always points into the direction of the largest variance of the object's points, and the magnitude of this vector equals the corresponding eigenvalue, λ_1 . The second largest eigenvector, \vec{v}_2 , is always orthogonal to the largest eigenvector, and points into the direction of the second largest spread of the data. Therefore, the first two axes, X and Y, are defined by the eigenvectors \vec{v}_1 and \vec{v}_2 , respectively. However, regarding the third axis, Z, instead of defining it based on \vec{v}_3 , we define it based on the cross product $\vec{v}_1 \times \vec{v}_2$. The object is then transformed to be placed in the reference frame.

Afterwards, we use an orthographic projection method to generate views of the object. It is worth to mention that the orthographic projection is a universal language among people in engineering professions and uses for technical drawing. In orthographic projection, up to six views of an object can be produced (called primary views). In this work, we just use three projection views including *front*, *top*, *right-side* and do not consider the *rear*, *bottom* and *left-side* views since they are mirror of the considered views, and do not contain new information about the object. In this method, since projection lines are parallel to each other and are perpendicular to the projection plane, an accurate outline of the visible face of the object is obtained. We therefore create three square projection planes centered on the object's center. Each plane of projection is positioned between the observer and the object and is perpendicular to one axis and parallel with the others axes of the object reference frame. The side length of projection planes, l , is determined by the largest edge length of a tight-fitting axis-aligned bounding box (AABB) of the object. This choice makes the projections scale invariant. The dimensions of the AABB are obtained by computing the minimum and maximum coordinate values along each axis. The object is then projected on the planes (see Fig.1).

As depicted in Fig. 2 the direction of eigenvectors is

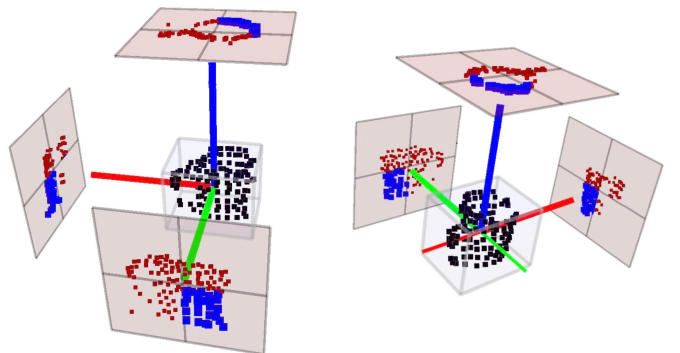


Fig. 2. Visualization of sign disambiguation procedure: The red, green and blue lines represent the unambiguous X, Y, Z axes respectively. Two orthographic projections of the object on the XoZ and YoZ planes are used to determine the sign of X and Y axis respectively; (left) sign is positive and; (right) sign is negative, and therefore all projections have been mirrored. For a better representation, we highlighted the corresponding bins of projections.

not unique, i.e., not repeatable across different trials and its orientation has 180° ambiguity. Therefore, the orthographic projections can be mirrored. This problem is known as the *sign ambiguity*, for which there is no mathematical solution [2]. To cope with this issue, it is suggested that the sign of each axis be similar to the sign of the Pearson’s correlation of the scatter points. For building a scatter plot, each projected point $\rho = (\alpha, \beta) \in R^2$, where α is the perpendicular distance to the horizontal axis and β is the perpendicular distance to the vertical axis, is then shifted to right and top by $\frac{1}{2}$. To complete the disambiguation, Pearson’s correlation, r , is computed for the XoZ projection plane to find the direction of X axis:

$$r_x = \frac{\sum \alpha_i \beta_i - n \bar{\alpha} \bar{\beta}}{\sqrt{(\sum \alpha_i^2 - n \bar{\alpha}^2)} \sqrt{(\sum \beta_i^2 - n \bar{\beta}^2)}}. \quad (2)$$

where $\bar{\alpha}$ and $\bar{\beta}$ are the mean of α and β . In particular, Pearson’s correlation reflects the non-linearity and direction of a linear relationship as a value between -1 and 1, where 1 indicates a strong positive relationship, -1 indicates a strong negative relationship. A similar indication, r_y , is computed for the Y axis using YoZ plane. Finally, the sign of the axes is determined as $s = r_x \cdot r_y$, where s can be either positive or negative. In the case of negative s , the three projections should be mirrored otherwise not (see Fig. 2).

Afterwards, the obtained projection views are uniformly scaled to an appropriate input image size and then fed into a CNN, pre-trained on ImageNet, to extract view-wise features. Finally, the obtained CNN features are merged using an element-wise max-pooling function to generate a global representation for the given object. In particular, our approach supports rotation invariant by employing a unique and repeatable global object reference frame together with a max/avg pooling layer. An illustrative example of the object representation procedure is depicted in Fig. 1.

IV. OBJECT CATEGORY LEARNING AND RECOGNITION

Object recognition using limited training data, is crucial for robotics applications and attracted interests in the research community recently. In a real-world application, the robot must learn about novel object categories from very few examples online e.g., when a user is defining a category “*on-the-fly*” using specific examples. In such scenarios, CNNs dramatically overfit to the training data and are not able to work properly. We have tackled this problem by proposing an instance-based learning and recognition (IBL) approach which considers category learning as a process of learning about the instances of the category, i.e., a category is represented simply by a set of known instances, $C \leftarrow \{\mathbf{O}_1, \dots, \mathbf{O}_n\}$, where \mathbf{O}_i are the constituent views. IBL is a baseline approach to evaluate object representations. An advantage of the IBL approaches is that they can recognize objects using a very small number of experiments and the training phase is very fast. In our current setup, a new instance of a specific category is stored in the robot’s memory in the following situations:

- When the teacher for the first time teaches a certain category, through a *Teach* or a *Correct* action, an instance-based representation of this new category is created and initialized with the set of views of the target object collected since object tracking started:

$$C_1 \leftarrow \{\mathbf{O}_1, \dots, \mathbf{O}_{1k_1}\}, \quad (3)$$

where k_1 is the number of stored key object views for the first teaching action.

- In later teaching actions, the target object views are added to the instance-based representation of the category:

$$C_n \leftarrow C_{n-1} \cup \{\mathbf{O}_{nk}, \dots, \mathbf{O}_{1k_n}\}, \quad (4)$$

where k_n is the number of stored key object views for the n -th teaching action.

Whenever a new object is added to a category, the agent retrieves the current model of the category and updates the category model by storing the representation of new object views. In particular, our approach can be seen as a combination of a particular *object representation*, *similarity measure* and *classification rule*. Therefore, the choice of the similarity metric has an impact on the recognition performance.

In the case of similarity measure, since the proposed object representation describes an object as a feature vector, the dissimilarity between two feature vectors can be computed by different distance functions. We refer the reader to a comprehensive survey on distance/similarity measures provided by S. Cha [3]. After performing several cross-validation experiments, we conclude two type of distance functions including Jensen-Shannon (JS) and chi-squared (χ^2) distances are suitable to estimate the similarity between two instances. Both functions are in the form of a bin-to-bin distance function. Although the practical results of χ^2 and JS are almost identical, χ^2 is computationally more efficient. Therefore, we use χ^2 function to estimate the similarity of two instances. Mathematically, let P and Q $\in \mathbb{R}^K$ be the representation of two objects:

$$\chi^2(P, Q) = \frac{1}{2} \sum_{i=1}^K \frac{(P_i - Q_i)^2}{(P_i + Q_i)}. \quad (5)$$

To assess the dissimilarity between a target object and stored instances of a certain category C, the minimum distance between the target object and all stored instances of the category C is considered as the Object-Category-Distance (OCD). The target object is finally classified based on the minimum OCD.

V. RESULT AND DISCUSSION

Three types of experiments were performed to evaluate the proposed approach.

A. Off-Line Evaluation

As depicted in Fig. 1, our approach uses three CNNs to generate a global deep representation from the three orthographic projections of the given object. In this approach, the resolution

of orthographic projections and the CNN architecture must be well selected to provide a good balance among recognition performance, computation time and memory usage. To define the optimal system configuration, we conduct 14 sets of evaluations using various CNN architectures, pre-trained on ImageNet dataset. For each CNN, 18 experiments were performed for different resolutions of orthographic images ranging from 25×25 to 225×225 pixels and two pooling functions including average and max pooling.

1) **Dataset and evaluation metrics:** The offline evaluations were carried out on using *Princeton ModelNet10* dataset [39], which consists of 4899 3D models split into 3991 training samples and 908 testing samples from 10 categories. Since ModelNet10 has a small number of classes with the significant intra-class variation that is suitable for performing extensive sets of experiments. We mainly report the results as average instance / class accuracy. Average instance accuracy (AIA) counts the percentage of the correctly recognized testing instances among all the testing instances, whereas the average class accuracy (ACA) is the average accuracy of all the categories.

2) **Results:** A set of experiments was carried out to evaluate the performance of the proposed approach concerning 3D object classification. A summary of the experiments is plotted in Fig. 3 (*top-row*). In these experiments, the best ACA results were obtained with *MobileNet-v2*, *average pooling* and image resolution of 150×150 pixels. The accuracy of the proposed system with this configuration was 0.8685. The ACA of the system with the same configuration and *max pooling* was 0.8678 percent. Although a high resolution orthographic image provides more details about the point distribution, it increases computation time, memory usage and sensitivity to noise. Therefore, we use *MobileNet-v2* and set image resolution to 150×150 pixels and use *average pooling* by default. As it can be observed from Fig. 3 (*top-row*), the descriptiveness of *DenseNet* architectures [14] (i.e., 121, 169, 201) is the worst among the evaluated CNNs. We realized that several misclassifications mainly occurred among items that look alike. In particular, some instances in the *desk* category has a very similar shape to the instances of *table* category; similarly, there are several highly similar instances in *dresser* and *night_stand* categories.

Overall, the top-three CNNs are *MobileNet-v2*, *VGG16-fc1* [32] and *ResNet50* [12] which achieved a good average class accuracy with stable performance. It is worth to mention, the length of feature vector, size and depth of the CNN architecture have direct influence on memory usage and computation time in both learning and recognition phases. Table I summarizes the proprieties of the top-three CNNs.

TABLE I
PROPRIETIES OF THE TOP-THREE CNNs.

Model	Feature Length	Size	#Parameters	Depth
MobileNet-v2	1280 float	14 MB	3.53 M	88
VGG16	4096 float	528 MB	138.35 M	23
ResNet50	4096 float	99 MB	25.63 M	168

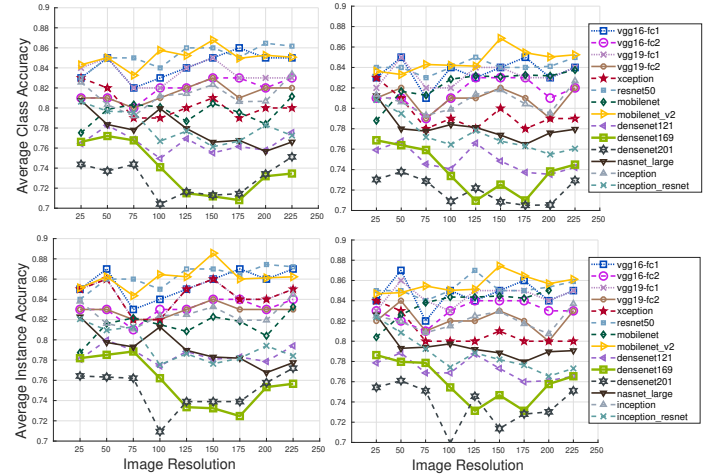


Fig. 3. Summary of off-line evaluations using various CNN architectures and two pooling functions: (*top-row*) average class accuracy vs. image resolution; (*bottom-row*) average instance accuracy vs. image resolution; (*left-column*) results using max pooling; (*right-column*) results using average pooling.

The length of feature extracted by *MobileNet-v2* is 1280 float, while both *VGG16-fc1* and *ResNet50* represent an object by a vector of 4096 float. The size of *MobileNet-v2* is 14MB which is around 37 and 7 times smaller than than *VGG16-fc1* and *ResNet50* respectively. According to this evaluations, our approach with *MobileNet-v2* is competent for robotic applications with strict limits on the memory footprint and computation time requirements.

We performed another set of experiments to evaluate our approach in the case of 3D object retrieval. Fig. 3 (*bottom-row*) compares the average instance accuracy of the evaluated system configurations in which several observations can be made. First, similar to the previous round of experiments, our approach with *MobileNet-v2*, *VGG16-fc1* and *ResNet50* demonstrated a good performance. In contrast, the AIA of DenseNets was lower than the others under all level levels of image resolution. The other evaluated CNNs, including *Xception* [5], *Nasnet* [41], *Inception* [36] and *Inception_Resnet* [37], demonstrated a medium-level performance. The parameters that obtained the best accuracy were selected as the default system parameters. Overall, the best AIA obtained with *MobileNet-v2*, *max pooling* and orthographic projections with the resolution of 150×150 pixels which was 88.56 percent. Besides, the AIA of the system with the same configuration and *average pooling* was 87.44. It is worth to mention, alternative pooling functions, e.g., *sum / min pooling*, lead to worse accuracy. This evaluation shows that the overall performance of the proposed approach is promising and it is capable of providing distinctive global features for 3D objects.

We have compared our method with five recent state-of-the-art approaches including ShapeNet [39], DeepPano [31], GeometryImage [33], BeamNet [40] and PointNet [10]. Table II presents a summary of the obtained results. It was observed that the discriminative power of our approach concerning ACA was better than the other state-of-the-art approaches. Particularly, it was 18.59 percentage points (p.p.) better than ShapeNet, 2.74 p.p. better than

DeepPano, 11.95 p.p., and 9.25 p.p. better than GeometryImage and PointNet respectively. The AIA of ShapeNet and DeepPano was not as good as the other approaches.

TABLE II
RECOGNITION PERFORMANCE

Approach	Accuracy (%)	
	Instance	Class
ShapeNet	83.54	68.26
DeepPano	85.45	84.18
GeometryImage	88.40	74.90
BeamNet	88.00	—
PointNet	—	77.60
Our work	88.56	86.85

orthographic projection, therefore less affected by noise.

B. Open-Ended Evaluation

Another round of experiments was carried, using the standard teaching protocol [15, 4] to evaluate open-ended learning approaches, concerning their scalability with respect to the number of learned categories. The idea is to emulate the interactions of a robot with the surrounding environment over significant periods of time. This protocol is based on a Test-then-Train scheme, which can be followed by a human user or by a simulated user. We developed a *simulated user* to follow the protocol and autonomously interact with the system. The idea is that for each newly taught category, the simulated teacher repeatedly picks unseen object views of the currently known categories from a dataset and presents them to the system. It progressively estimates the recognition accuracy of the system and, in case this accuracy exceeds a given threshold ($\tau = 0.67$, meaning accuracy is at least twice the error rate), introduces an additional object category. This way, the system is trained online, and at the same time, the accuracy of the system is continuously estimated. In case the agent can not reach the classification threshold after a certain number of iterations (i.e., 100 iterations), the simulated teacher can infer that the agent is no longer able to learn more categories and terminates the experiment. It is possible that the agent learns all existing categories before reaching to the breaking points. In such cases, it is no longer possible to continue the protocol, and the evaluation process is halted. In the reported results, this is shown by the stopping condition, “*lack of data*”.

1) *Dataset and evaluation metrics*: The Washington RGB-D Object dataset [21] is used for open-ended evaluation since it is a large scale dataset concerning the number of images. It consists of 250,000 views of 300 common manipulable household objects taken from multiple views and organized into 51 categories. We evaluate our experimental results using the metrics that was recently introduced in [24], including: (i) the number of learned categories at the end of an experiment (TLC), an indicator of *how much the system is capable of learning*; (ii) the number of question/correction iterations (QCI) required to learn those categories and the average number of stored instances per category (AIC), indicators of *time and memory resources required for learning*; (iii) Global Classification Accuracy (GCA), an accuracy computed using

Our work, GeometryImage and BeamNet obtained promising AIA performance. The fact that our approach is computed on an stable, unique and unambiguous loca reference frame is likely to explain the obtained results.

Furthermore, our approach uses three

TABLE III
SUMMARY OF OPEN-ENDED EVALUATION.

Approaches	#QCI	ALC	AIC	GCA	APA
RACE [25]	382.10	19.90	8.88	0.67	0.78
BoW [17]	411.80	21.80	8.20	0.71	0.82
Open-Ended LDA [13]	262.60	14.40	9.14	0.66	0.80
Local-LDA [19]	613.00	28.50	9.08	0.71	0.80
GOOD [18]	1659.20	39.20	17.28	0.66	0.74
ours+ <i>MobileNet-v2</i> ^(*)	1342.60	51.00	8.97	0.77	0.80
ours+ <i>VGG16-fc1</i> ^(#)	1568.70	48.10	12.42	0.71	0.76
ours+ <i>ResNet50</i> ^(#)	1446.60	51.00	10.21	0.75	0.78

^(*) Stopping condition was “*lack of data*”. ^(#) In 6 out of 10 experiments, stopping condition was “*lack of data*”

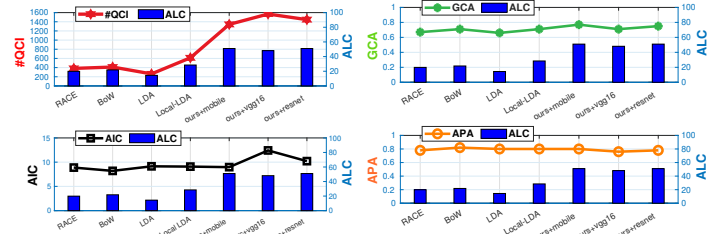


Fig. 4. Summary of open-ended evaluations.

all predictions in a complete experiment, and the Average Protocol Accuracy (APA), indicators of *how well the system learns*. Since the order in which categories are introduced may have an effect on the performance of the system, ten experiments were carried out for each approach.

2) *Results*: We have conducted an extensive comparison with five open-ended 3D object category learning and recognition approaches, including RACE [25], BoW [17] using a L_2 based nearest neighbour classifier, Open-ended LDA, which is a modified version of the standard online LDA [13], Local-LDA [19] and GOOD [18]. Furthermore, since our approach with *MobileNet-v2*, *VGG16-fc1* and *ResNet50* demonstrated a good performance in previous round of evaluation, we have included all of them in this round of evaluation. A detailed summary of the obtained results is reported in Fig. 4 and the Table III.

Fig. 4 (*top-left*) illustrates *how fast* the learning occurred in each of the experiments. It shows the number of question/correction iterations (QCI) required to learn a certain number of categories. We see that on average the longest experiments were observed with our approach using *VGG16-fc1* and the shortest ones were observed with Open-Ended LDA. In the case of Open-Ended LDA, the agent on average learned 14.40 categories using 262.60 question/correction iterations. *VGG16-fc1* based approach on average continued for 1568.70 question/correction iterations and the agent was able to learn 48.10 categories. It is also visible that the agent learned (on average) more categories using our approaches than with other approaches. One important observation is that our approach with *MobileNet* and *ResNet50* learned all 51 categories in all 10 experiments and all experiments concluded prematurely due to the “*lack of data*”, i.e., no more categories available in the dataset, indicating the potential for learning many more categories. Our *VGG16-fc1* based approach also obtained an

acceptable scalability (i.e., in six out of 10 experiments, the agent could learn all categories) while the scalability of other approaches were much lower. Our approach with *MobileNet* on average can learn all the categories faster than the other approaches.

By comparing all approaches, it is clear that RACE, BoW and our work with *MobileNet-v2* on average stored less than nine instance per category. Although, RACE and BoW approaches stored fewer instances per category (AIC), than our approach, the difference is minor (less than one instance per category) and the discriminative power of those two approaches is lower (see Fig. 4 *bottom-left*). In particular, our approach learned 31.10 and 29.20 categories more than RACE and BoW approaches, respectively.

The right column of Fig. 4 correlates the global classification accuracy (GCA, *top-right*) and average protocol accuracy (APA, *bottom-right*), obtained by the evaluated approaches, with the average number of learned categories (ALC). Our approach with *MobileNet-v2* achieved the best GCA with stable performance. BoW achieved better performance than our approaches regarding APA. This is expected since BoW learned fewer categories, and it is easier to get better APA in fewer categories. In particular, our approach with *MobileNet-v2* was able to learn all 51 categories, on average, while the other approaches learned less than 40 categories. It can be concluded from this evaluations that our approach with *ModelNet-v2* achieved the best performance.

C. Demonstration

To show the strength of the proposed approach, we carried out two types of demonstration. For both demonstrations, the proposed approach has been integrated into the object perception system presented in [25].

1) *Scene dataset*: We report on a demonstration using the Imperial College Domestic Environment Dataset[8]. This is a suitable dataset for this test since all scenes were captured under various clutter and contain several objects. In this demonstration, the system initially had no prior knowledge, and all objects are recognized as unknown. Later, a user interacts with the system in an online manner and teaches all object categories including *amita*, *colgate*, *lipton*, *elite*, *oreo* and *softkings* to the system using the objects extracted from scenes captured from the blue cameras as shown in Fig. 5 (*top-left*). The system conceptualizes those categories using the extracted object views. Afterwards, the system is tested by the remaining ten scenes captured from different viewpoints (i.e., shown by red cameras). The system could recognize all objects properly by using the knowledge learned from the first three scenes. Some misclassification also occurred throughout the demonstration. The underlying reason was that, at some points, the object tracking could not track the object accurately and the distinctive parts of the object were not included in the object’s point cloud. An example of results is depicted in Fig. 5 (*top-right*).

Later, we moved the system to two new contexts, where the first context contains six instances of three categories including

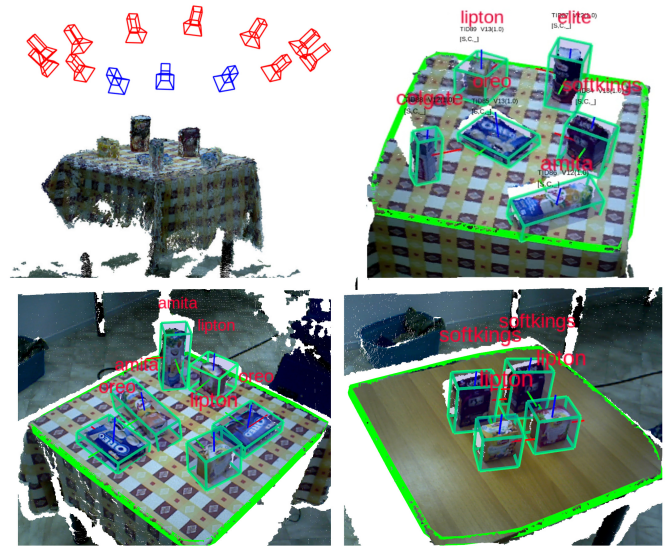


Fig. 5. Real demonstration using Imperial College Domestic Environment dataset: (*top-left*) Experimental setup: we train the robot using the objects’ views extracted from the scenes captured from the blue cameras. We then test the robot using the remaining scenes captured from the red cams. (*top-right*) a snapshot of the object recognition results for the first test scene; (*bottom-left*) we also test the system using another scene, where six instances of the three categories exist; this shows the rotation invariant property since both *amita* cases have been recognized correctly; (*bottom-right*) The system can accurately distinguish “*lipton*” from “*softkings*”; this snapshot shows the descriptive power of the proposed approach.

oreo, *amita*, and *lipton*. The robot could recognize all objects correctly by using knowledge from the previous environment. In this scene, we showed the rotation invariant property of the *OrthographicNet* since both *amita* instances have been recognized correctly (see Fig. 5 *bottom-left*). The second context comprises four instances of two object categories with very similar shapes (*lipton* vs. *softkings*). The system could recognize all objects properly by using the learned knowledge. This demonstration shows the descriptive power of the proposed approach. Overall, this evaluation illustrates the process of learning object categories in an open-ended fashion. A video of this demonstration is available online at: <https://youtu.be/JEUb-Q7TbJQ>

2) “*Serve A Drink*” *scenario*: In this demonstration, a table is in front of a Kinect sensor, and a user interacts with the system (see Fig.6 *top-left*). Initially, the system has prior knowledge about *juiceBox* and *oreo*, learned from batch data (i.e., set of observations with ground truth labels), and does not have any information about the *bottle* and *cup* categories. Figure 6 and the following description explains the behavior of the proposed approach:

- The user presents a *cup* object to the system and provides the respective category labels (TrackID9 as a *cup*). The system conceptualizes the *cup* category and TrackID9 is correctly recognized.
- The instructor places a *juiceBox* on the table. The system has learned about *juiceBox* category from batch data, therefore, TrackID10 is recognized properly. An additional *juiceBox* is placed at the left-side of the table.

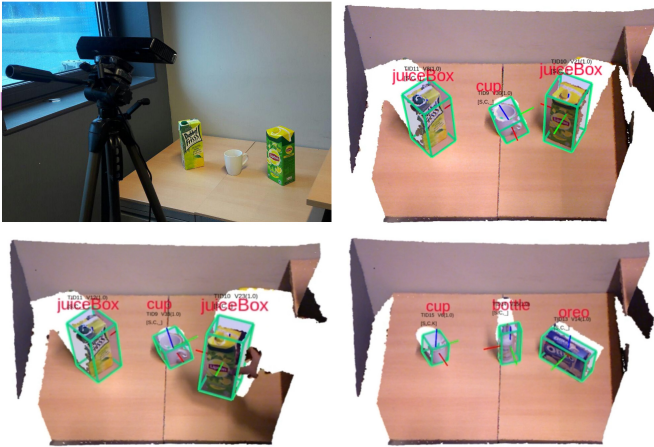


Fig. 6. A real-time system demonstration – *serve_a_drink* scenario – : (top-left) experimental setup; (top-right) This snapshot shows the proposed system supports both classical (i.e., learning from a batch of labeled training data) and open-ended learnings; the system gained knowledge about *juiceBox* using batch learning and learns about *cup* category using on-line experiences in open-ended manner; (bottom-left) a user moves the *juiceBox* and the system can track and recognize it correctly; (bottom-right) the user then removes all objects from the table and adds three new objects including *oreo*, *bottle* and a new *cup*. The system had prior knowledge about *oreo*; it also learns about *bottle* category in an online manner and recognizes all object correctly.

Tracking is initialized and the *juiceBox* is recognized accurately (Fig. 6 top-right).

- The instructor moves the right *juiceBox* for a while to show the real-time performance of the *OrthographicNet* for performing object recognition and pose estimation concurrently (Fig. 6 bottom-left).
- Later, the user removes all objects from the scene; no objects are visible; an *oreo* and a *bottle* enter the scene. They are detected and assigned to TrackID13 and TrackID14 respectively. Because there is no prior knowledge about *bottle* category, a misclassification happened. TrackID14 is labelled as a *bottle*; the system first conceptualizes the *bottle* category and then recognizes it correctly.
- Another *cup* is placed on the table. This particular *cup* had not been previously seen, but it recognizes correctly since the system learned about *cup* category earlier (Fig. 6 bottom-right).

This demonstration shows that apart from batch learning, the robot can also learn about new object categories in an open-ended fashion. Furthermore, it shows that the proposed approach is capable of recognizing objects in various positions. A video of this demonstration is available online at: <https://youtu.be/09UK4IxbRH4>

VI. CONCLUSION

In this paper, we propose a deep transfer learning based approach for 3D object recognition in open-ended domains named *OrthographicNet*. This approach provides a good trade-off between descriptiveness, computation time and memory usage, allowing concurrent object recognition and pose estimation. *OrthographicNet* computes a unique and repeatable global object reference frame and three scale-invariant orthographic projections for a given object. The orthographic

projects are then fed as input to three modern CNN architectures to obtain a view-wise deep feature. The obtained features are then merged using an element-wise max pooling layer to form a global rotation-invariant feature for the object. A set of experiments were carried out to assess the performance of *OrthographicNet* and compare it with other state-of-art with respect to several characteristics including descriptiveness, scalability and memory usage. We have shown that *OrthographicNet* can achieve performance better than the selected state-of-the-art. The overall average class accuracy obtained with *OrthographicNet* is comparable to the best performances obtained with the state-of-the-art approaches. *OrthographicNet* is especially suited for real-time robotic applications. We plan to release the source code of this work to the benefit of the research community in the near future. In the continuation of this work, we would like to investigate the possibility of using orthographic projections for recognizing 3D object category and grasp affordance concurrently.

REFERENCES

- [1] Aitor Aldoma, Zoltan-Csaba Marton, Federico Tombari, Walter Wohlkinger, Christian Potthast, Bernhard Zeisl, Radu Bogdan Rusu, Suat Gedikli, and Markus Vincze. Tutorial: Point cloud library: Three-dimensional object recognition and 6 dof pose estimation. *IEEE Robotics & Automation Magazine*, 19(3):80–91, 2012.
- [2] Rasmus Bro, Evrim Acar, and Tamara G Kolda. Resolving the sign ambiguity in the singular value decomposition. *Journal of Chemometrics: A Journal of the Chemometrics Society*, 22(2):135–140, 2008.
- [3] Sung-Hyuk Cha. Comprehensive survey on distance/similarity measures between probability density functions. *International Journal of Mathematical Models and Methods in Applied Sciences*, 1(4):300–307, 2007.
- [4] Aneesh Chauhan and Luís Seabra Lopes. Using spoken words to guide open-ended category formation. *Cognitive processing*, 12(4):341, 2011.
- [5] François Chollet. Xception: Deep learning with depth-wise separable convolutions. *arXiv preprint*, pages 1610–02357, 2017.
- [6] Taco Cohen and Max Welling. Group equivariant convolutional networks. In *International conference on machine learning*, pages 2990–2999, 2016.
- [7] Sander Dieleman, Jeffrey De Fauw, and Koray Kavukcuoglu. Exploiting cyclic symmetry in convolutional neural networks. *arXiv preprint arXiv:1602.02660*, 2016.
- [8] Andreas Doumanoglou, Rigas Kouskouridas, Sotiris Malassiotis, and Tae-Kyun Kim. Recovering 6d object pose and predicting next-best-view in the crowd. In *Proceedings of the IEEE Conference on Computer Vision and Pattern Recognition*, pages 3583–3592, 2016.
- [9] Thomas F aulhammer, Rares Ambrus, Christopher Burbridge, Micheal Zillich, John Folkesson, Nick Hawes, Patric Jensfelt, and Marcus Vincze. Autonomous learning

- of object models on a mobile robot. *IEEE Robotics and Automation Letters*, 2(1):26–33, 2017.
- [10] Alberto Garcia-Garcia, Francisco Gomez-Donoso, Jose Garcia-Rodriguez, Sergio Orts-Escolano, Miguel Cazorla, and J Azorin-Lopez. Pointnet: A 3d convolutional neural network for real-time object class recognition. In *Neural Networks (IJCNN), 2016 International Joint Conference on*, pages 1578–1584. IEEE, 2016.
- [11] Ian Goodfellow, Jean Pouget-Abadie, Mehdi Mirza, Bing Xu, David Warde-Farley, Sherjil Ozair, Aaron Courville, and Yoshua Bengio. Generative adversarial nets. In *Advances in neural information processing systems*, pages 2672–2680, 2014.
- [12] Kaiming He, Xiangyu Zhang, Shaoqing Ren, and Jian Sun. Deep residual learning for image recognition. In *Proceedings of the IEEE conference on computer vision and pattern recognition*, pages 770–778, 2016.
- [13] Matthew Hoffman, Francis R Bach, and David M Blei. Online learning for latent dirichlet allocation. In *advances in neural information processing systems*, pages 856–864, 2010.
- [14] Gao Huang, Zhuang Liu, Laurens Van Der Maaten, and Kilian Q Weinberger. Densely connected convolutional networks. In *2017 IEEE Conference on Computer Vision and Pattern Recognition (CVPR)*, pages 2261–2269. IEEE, 2017.
- [15] S Hamidreza Kasaei, Miguel Oliveira, Gi Hyun Lim, Luis Seabra Lopes, and Ana Maria Tome. Interactive open-ended learning for 3d object recognition: An approach and experiments. *Journal of Intelligent & Robotic Systems*, 80(3-4):537–553, 2015.
- [16] S Hamidreza Kasaei, Ana Maria Tomé, Luis Seabra Lopes, and Miguel Oliveira. Good: A global orthographic object descriptor for 3d object recognition and manipulation. *Pattern Recognition Letters*, 83:312–320, 2016.
- [17] S Hamidreza Kasaei, Miguel Oliveira, Gi Hyun Lim, Luís Seabra Lopes, and Ana Maria Tomé. Towards lifelong assistive robotics: A tight coupling between object perception and manipulation. *Neurocomputing*, 291:151–166, 2018.
- [18] S Hamidreza Kasaei, Juil Sock, Luis Seabra Lopes, Ana Maria Tomé, and Tae-Kyun Kim. Perceiving, learning, and recognizing 3d objects: An approach to cognitive service robots. In *Thirty-Second AAAI Conference on Artificial Intelligence*, 2018.
- [19] Seyed Hamidreza Kasaei, Ana Maria Tomé, and Luís Seabra Lopes. Hierarchical object representation for open-ended object category learning and recognition. In *Advances in Neural Information Processing Systems*, pages 1948–1956, 2016.
- [20] Roman Klokov and Victor Lempitsky. Escape from cells: Deep kd-networks for the recognition of 3d point cloud models. In *Computer Vision (ICCV), 2017 IEEE International Conference on*, pages 863–872. IEEE, 2017.
- [21] Kevin Lai, Liefeng Bo, Xiaofeng Ren, and Dieter Fox. A large-scale hierarchical multi-view rgb-d object dataset. In *Robotics and Automation (ICRA), 2011 IEEE International Conference on*, pages 1817–1824. IEEE, 2011.
- [22] David G Lowe. Object recognition from local scale-invariant features. In *Computer vision, 1999. The proceedings of the seventh IEEE international conference on*, volume 2, pages 1150–1157. Ieee, 1999.
- [23] Daniel Maturana and Sebastian Scherer. Voxnet: A 3d convolutional neural network for real-time object recognition. In *Intelligent Robots and Systems (IROS), 2015 IEEE/RSJ International Conference on*, pages 922–928. IEEE, 2015.
- [24] Miguel Oliveira, Luís Seabra Lopes, Gi Hyun Lim, S Hamidreza Kasaei, Angel D Sappa, and Ana Maria Tomé. Concurrent learning of visual codebooks and object categories in open-ended domains. In *Intelligent Robots and Systems (IROS), 2015 IEEE/RSJ International Conference on*, pages 2488–2495. IEEE, 2015.
- [25] Miguel Oliveira, Luís Seabra Lopes, Gi Hyun Lim, S Hamidreza Kasaei, Ana Maria Tomé, and Aneesh Chauhan. 3d object perception and perceptual learning in the race project. *Robotics and Autonomous Systems*, 75:614–626, 2016.
- [26] Charles R. Qi, Hao Su, Matthias Niessner, Angela Dai, Mengyuan Yan, and Leonidas J. Guibas. Volumetric and multi-view cnns for object classification on 3d data. In *The IEEE Conference on Computer Vision and Pattern Recognition (CVPR)*, June 2016.
- [27] Charles Ruizhongtai Qi, Li Yi, Hao Su, and Leonidas J Guibas. Pointnet++: Deep hierarchical feature learning on point sets in a metric space. In *Advances in Neural Information Processing Systems*, pages 5099–5108, 2017.
- [28] Samuele Salti, Federico Tombari, and Luigi Di Stefano. Shot: Unique signatures of histograms for surface and texture description. *Computer Vision and Image Understanding*, 125:251–264, 2014.
- [29] Ali Sharif Razavian, Hossein Azizpour, Josephine Sullivan, and Stefan Carlsson. Cnn features off-the-shelf: an astounding baseline for recognition. In *Proceedings of the IEEE conference on computer vision and pattern recognition workshops*, pages 806–813. IEEE, 2014.
- [30] Ali Sharif Razavian, Hossein Azizpour, Josephine Sullivan, and Stefan Carlsson. Cnn features off-the-shelf: an astounding baseline for recognition. In *Proceedings of the IEEE conference on computer vision and pattern recognition workshops*, pages 806–813. IEEE, 2014.
- [31] Baoguang Shi, Song Bai, Zhichao Zhou, and Xiang Bai. Deeppano: Deep panoramic representation for 3-d shape recognition. *IEEE Signal Processing Letters*, 22(12): 2339–2343, 2015.
- [32] Karen Simonyan and Andrew Zisserman. Very deep convolutional networks for large-scale image recognition. *arXiv preprint arXiv:1409.1556*, 2014.
- [33] Ayan Sinha, Jing Bai, and Karthik Ramani. Deep learning 3d shape surfaces using geometry images. In *European Conference on Computer Vision*, pages 223–240. Springer, 2016.

- [34] Danijel Skočaj, Alen Vrečko, Marko Mahnič, Miroslav Janiček, Geert-Jan M Kruijff, Marc Hanheide, Nick Hawes, Jeremy L Wyatt, Thomas Keller, Kai Zhou, et al. An integrated system for interactive continuous learning of categorical knowledge. *Journal of Experimental & Theoretical Artificial Intelligence*, 28(5):823–848, 2016.
- [35] Hang Su, Subhansu Maji, Evangelos Kalogerakis, and Erik Learned-Miller. Multi-view convolutional neural networks for 3d shape recognition. In *Proceedings of the IEEE international conference on computer vision*, pages 945–953, 2015.
- [36] Christian Szegedy, Vincent Vanhoucke, Sergey Ioffe, Jon Shlens, and Zbigniew Wojna. Rethinking the inception architecture for computer vision. In *Proceedings of the IEEE conference on computer vision and pattern recognition*, pages 2818–2826, 2016.
- [37] Christian Szegedy, Sergey Ioffe, Vincent Vanhoucke, and Alexander A Alemi. Inception-v4, inception-resnet and the impact of residual connections on learning. In *AAAI*, volume 4, page 12, 2017.
- [38] Yu-Xiong Wang, Ross Girshick, Martial Hebert, and Bharath Hariharan. Low-shot learning from imaginary data. *arXiv preprint arXiv:1801.05401*, 2018.
- [39] Zhirong Wu, Shuran Song, Aditya Khosla, Fisher Yu, Linguang Zhang, Xiaoou Tang, and Jianxiong Xiao. 3d shapenets: A deep representation for volumetric shapes. In *Proceedings of the IEEE conference on computer vision and pattern recognition*, pages 1912–1920, 2015.
- [40] Xu Xu and Sinisa Todorovic. Beam search for learning a deep convolutional neural network of 3d shapes. *arXiv preprint arXiv:1612.04774*, 2016.
- [41] Barret Zoph, Vijay Vasudevan, Jonathon Shlens, and Quoc V Le. Learning transferable architectures for scalable image recognition. In *Proceedings of the IEEE conference on computer vision and pattern recognition*, pages 8697–8710, 2018.